LETTER

doi:10.1038/nature11339

Room-temperature solid-state maser

Mark Oxborrow[1], Jonathan D. Breeze[2] & Neil M. Alford[2]

The invention of the laser has resulted in many innovations, and the device has become ubiquitous. However, the maser, which amplifies microwave radiation rather than visible light, has not had as large an impact, despite being instrumental in the laser's birth[1,2]. The maser's relative obscurity has mainly been due to the inconvenience of the operating conditions needed for its various realizations: atomic[3] and free-electron[4] masers require vacuum chambers and pumping; and solid-state masers[5], although they excel as low-noise amplifiers[6] and are occasionally incorporated in ultrastable oscillators[7,8], typically require cryogenic refrigeration. Most realizations of masers also require strong magnets, magnetic shielding or both. Overcoming these various obstacles would pave the way for improvements such as more-sensitive chemical assays, more-precise determinations of biomolecular structure and function, and more-accurate medical diagnostics (including tomography) based on enhanced magnetic resonance spectrometers[9] incorporating maser amplifiers and oscillators. Here we report the experimental demonstration of a solid-state maser operating at room temperature in pulsed mode. It works on a laboratory bench, in air, in the terrestrial magnetic field and amplifies at around 1.45 gigahertz. In contrast to the cryogenic ruby maser[6], in our maser the gain medium is an organic mixed molecular crystal, *p*-terphenyl doped with pentacene, the latter being photo-excited by yellow light. The maser's pumping mechanism exploits spin-selective molecular intersystem crossing[10] into pentacene's triplet ground state[11,12]. When configured as an oscillator, the solid-state maser's measured output power of around −10 decibel milliwatts is approximately 100 million times greater than that of an atomic hydrogen maser[3], which oscillates at a similar frequency (about 1.42 gigahertz). By exploiting the high levels of spin polarization readily generated by intersystem crossing in photo-excited pentacene and other aromatic molecules, this new type of maser seems to be capable of amplifying with a residual noise temperature far below room temperature.

To the best of our knowledge, no-one has previously attempted to make a zero-field maser[13] out of an optically pumped crystal of pentacene-doped *p*-terphenyl. Two further novel features of the device we report here are a microwave cavity containing a dielectric ring of sapphire, which supports a high-Q electromagnetic mode (where Q is the mode's quality factor), and a medical laser, designed for the treatment of vascular skin lesions, that is here used to deliver intense pulses of pump light into the pentacene:*p*-terphenyl maser crystal at its optimal absorption wavelength (~585 nm).

Because they are key components within many measurement and telecommunication devices and systems, there has been intensive research on low-noise amplifiers for the purpose of improving their performance and reducing their operating requirements[14]. As low-noise amplifiers, conventional solid-state masers[5] offer low residual noise temperatures[6] and, in contrast to microfabricated devices, are extremely rugged with respect to electromagnetic shock and overloading. Furthermore, they have low intermodulation distortion[6], so reducing interference from out-of-band signals, and low flicker noise[7], thus enabling precise measurements. The active material within a conventional solid-state maser is a dielectric crystal containing paramagnetic ions, for example ruby, that is maintained typically below 10 K and exposed (with exceptions[8,13]) to a strong d.c. magnetic bias field. Despite the inconvenience of these operating conditions, as well as competition from amplifiers based on cooled high-electron-mobility transistors (HEMTs)[15], ruby masers are used in deep-space communications[6]. They were used, for example, by NASA to receive images of the Solar System's outer planets and their moons from the Voyager space probes[16].

The lowest-noise semiconductor-based amplifiers at microwave frequencies, which today most often incorporate cooled HEMTs[15], suffer from a particular limitation. On cooling, the HEMT amplifier's residual noise temperature, although low enough for many applications, is difficult to reduce below a few kelvin[17]. Although this 'HEMT plateau' can be lowered somewhat by using lower device powers[18], it has motivated the successful development of amplifiers based on resonant superconducting interference devices[17], which offer substantially lower noise temperatures, albeit over more limited bandwidths. But with both HEMTs and such devices, the attainment of millikelvin noise temperatures demands subkelvin refrigeration, as supplied by a dilution refrigerator or its equivalent.

It is known why conventional solid-state masers[5,6] cannot be made to work at room temperature[19]. The most serious problem is that the rate of spin–lattice relaxation, $1/T_1$, and, thus, the microwave power required to saturate the maser's pump transition and, in turn, the required thermal cooling power of the maser's refrigerator, increase extremely rapidly with the absolute (lattice) temperature, T, of the maser crystal. For two-phonon (Raman) scattering off Kramers-type paramagnetic ions in a three-dimensional lattice well below its Debye temperature, this relaxation rate scales as T^9. A second problem is that, even if the maser's pump transition can be saturated by pumping hard, the population inversion and, hence, the maser crystal's gain scale as $I \times hf_{\mathrm{mas.}}/kT$, where $I \equiv f_{\mathrm{pump}}/2f_{\mathrm{mas.}} - 1$ is the inversion ratio[5], $f_{\mathrm{mas.}}$

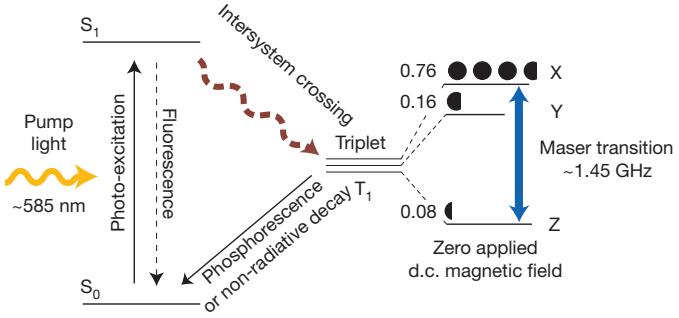

Figure 1 | Maser pumping scheme (Jablonski diagram). Pentacene guest molecules within a *p*-terphenyl host lattice are driven from their singlet ground states, S_0, into their first-excited single states, S_1, by absorbing photons of yellow pump light. From S_1, they predominantly undergo intersystem crossing into their triplet ground states, T_1. This process is spin selective; the relative population rates[11,12] (splitting ratios) into the three spin sublevels of T_1 are as stated (also represented by solid black circles). As can be seen, the uppermost sublevel, X, is preferentially populated, resulting in a strong initial population inversion between it and the lowest sublevel, Z, so providing the conditions for masing through the $X \leftrightarrow Z$ transition.

[1]National Physical Laboratory, Hampton Road, Teddington TW11 0LW, UK. [2]Imperial College, Department of Materials, South Kensington Campus, London SW7 2AZ, UK.

and f_{pump} are respectively the maser signal and pump frequencies, and k and h are respectively Boltzmann's and Planck's constants. The residual noise temperature of a conventionally pumped solid-state maser amplifier thus scales as T, so nullifying the maser's low-noise advantage at higher operating temperatures. It was realized very early on that, at the expense of energy efficiency, larger population inversions and, thus, lower noise temperatures and somewhat higher sustainable operating temperatures can be obtained, for a fixed $f_{mas.}$, by increasing f_{pump}—in the extreme case by driving optical pump transitions with light[20], which can often be supplied by a laser. But optical pumping alone does not obviate the first problem, that is, the rapid increase in the rate of spin–lattice relaxation with temperature[21].

Steps have been taken towards the realization of solid-state masers at room temperature using optically excited organic molecules in strong d.c. magnetic fields, focusing largely on C_{60} and porphyrins known to have long spin-polarization lifetimes[19] (T_1). But the 'triplet mechanism', of which Fig. 1 is an example, was considered unsuitable for maser operation at room temperature[22]. Maser threshold was almost reached by instead using the more complex, indirect, radical-triplet-pair mechanism (the triplet state in question being that of etioporphyrin); see fig. 3 of ref. 23. More recently, the potential of various triplet-mechanism photochemistries, including the fullerene derivative PCBM in polystyrene, was assessed in the context of realizing particle acceleration by stimulated emission of radiation at X-band microwave frequencies[24].

The maser reported here (Figs 1 and 2) is based on the triplet mechanism. It exploits spin-selective intersystem crossing[10] into the triplet ground state of pentacene molecules doping crystalline *p*-terphenyl[11], as has been studied in connection with realizations of both dynamic nuclear polarization[25] and electron spin resonance of single molecules[12]. On photo-excitation from pentacene's ground state, S_0, to its first excited singlet state, S_1, with yellow pump light (Fig. 1), intersystem crossing provides a strongly inverted spin population between the uppermost (X) and lowest (Z) spin sublevels of pentacene's triplet ground state[11,12]. The relatively high zero-field splitting (as compared with PCBM, for example) makes it practicable to use a microwave resonator with no applied d.c. magnetic field, which greatly simplifies the experiment set-up. Our chosen design of resonator (Fig. 2) is cylindrical and supports a frequency-tunable transverse-electric mode, $TE_{01\delta}$, which has no azimuthal dependence, has a single antinode in the radial and the axial directions, and has a mode volume of ~50 cm^3. With the pentacene:*p*-terphenyl crystal in place, this mode's unloaded quality factor (Q) was measured to be around 2×10^5. When critically coupled through a magnetic loop probe in the side of the resonator's enclosing metal can (Fig. 2), the mode offered a field-to-power conversion factor of $\Lambda \approx 5\ G\ W^{-1/2}$, which is proportional to the square root of the mode's magnetic Purcell factor[26].

An unpolarized, ~10-mm-diameter beam of yellow (585 ± 5 nm) pump light from a Candela SPTL-1b long-pulsed rhodamine-6G dye laser was directed at the maser crystal. This laser was capable of delivering up to 4 J of energy in a single pulse, at a rate of one pulse per second, although pulses of only 0.5 J were used in our experiment. (This pulse energy, the time-integrated power of the yellow trace in Fig. 3, was confirmed with a Molectron JMAX 43 pyroelectric joulemeter.) We estimate that ~0.3 J was absorbed in the maser crystal per pulse. With the frequency of the $TE_{01\delta}$ mode set near to the centre of the X↔Z spin transition, each pump pulse absorbed by the crystal produced a vigorous burst of maser oscillation (Fig. 3). The oscillation's magnitude as a function of the $TE_{01\delta}$ mode's frequency is shown in Fig. 4. The instantaneous output power of the maser burst (Fig. 3, blue trace), as monitored directly by a microwave receiver in the form of an HP8593E spectrum analyser set to fixed-frequency mode, was observed to exceed −10 dBm. Over 1,000 pump pulses, no change in the size or shape of the maser burst was noticeable provided that the resonator was kept in tune. By inserting neutral-density filters into the pump beam to extinguish the maser oscillation, the threshold pump energy exiting from the laser was determined to be 80 mJ over an effective pump pulse duration of 350 μs, which corresponds to a threshold pump power of about 230 W. Just above threshold, a considerably diminished maser burst, delayed in time and somewhat shorter in duration, could be observed.

We have constructed a simple model for how both the spin populations in the X and Z sublevels and the energization of (that is, photon number in) the maser mode change as functions of time in response to the applied optical pump pulse (Methods). The maser output power predicted by this model was fitted to the experimentally observed maser burst, yielding the green curve in Fig. 3, together with estimates of three spin-dynamics parameters. Our modelling suggests that near-zero-field operation is particularly advantageous for maser action (masing): the rate of spin–lattice relaxation is low and the transition linewidth is narrow[27].

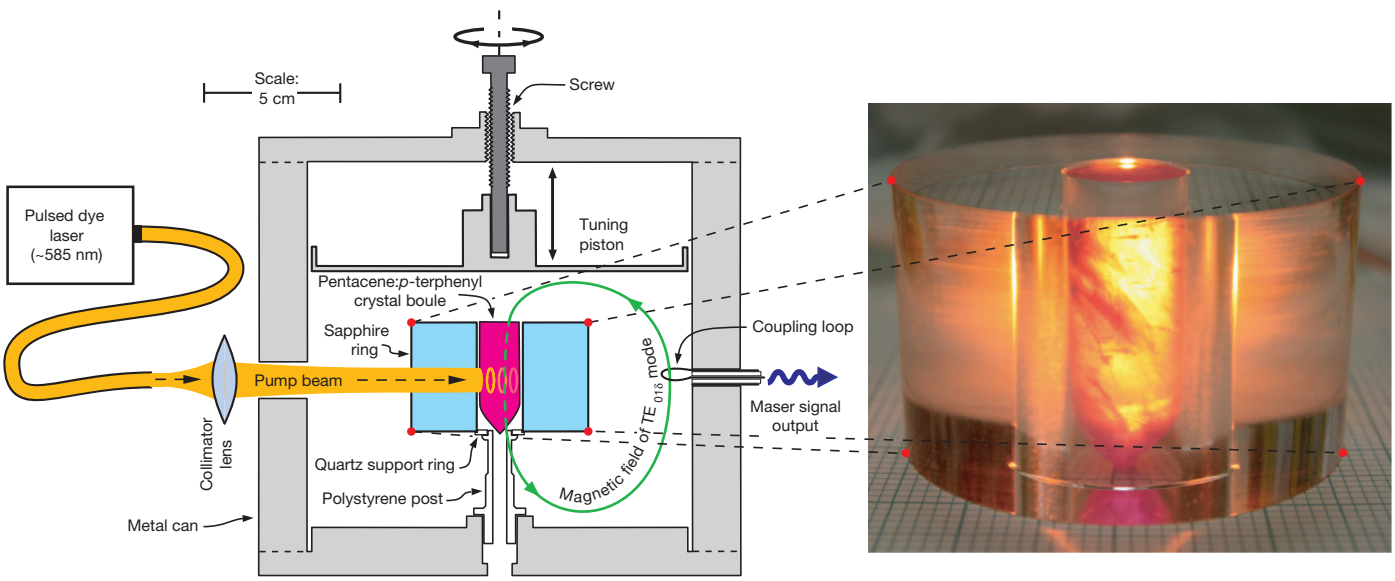

Figure 2 | Anatomy of the maser. A crystal of *p*-terphenyl doped with pentacene is located in the a.c. magnetic field of the $TE_{01\delta}$ mode of a microwave resonator and illuminated with a beam of yellow light from a pulsed dye laser. By maser action, the $TE_{01\delta}$ mode is energized, and from this mode a signal is extracted using a magnetic coupling loop. The photograph on the right shows the resonator's sapphire ring and the pentacene:*p*-terphenyl crystal slotted inside it; yellow back lighting reveals flaws within the crystal.

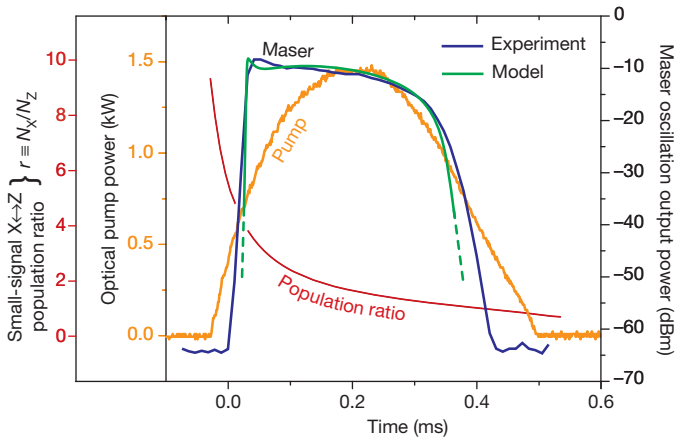

Figure 3 | Maser response in the time domain. The yellow trace (scale on near left) is the pump laser's instantaneous output power, which corresponds to an energy of ~0.5 J per pulse. The blue trace (scale on right) is the instantaneous power of the maser's oscillation burst as monitored with a microwave receiver at a resolution bandwidth of 10 MHz centred on 1.45 GHz. The green trace (same scale on right) is our fitted model's prediction of this instantaneous power. The red curve (scale on far left) is the predicted population ratio between the uppermost (X) and lowest (Z) maser levels in response to the optical pump in the low-signal regime.

Our experimental maser oscillator (Fig. 2) can be reconfigured as a pulsed-mode amplifier of weak electromagnetic signals by connecting its coupling loop to one port of a circulator[5]. A detailed, quantitative analysis of this amplifier's noise performance, taking into account deleterious sources of noise associated with losses within this circulator and the maser cavity itself, is provided in Methods. The red curve in Fig. 3 shows the population ratio $r \equiv N_X/N_Z$ between the uppermost (X) and lowest (Z) maser levels as predicted by our fitted model in response to the optical pump pulse shown (yellow trace). Whereas the blue and green curves correspond to saturation-limited maser oscillation, this red curve corresponds to the low-signal regime, where the energization of the maser mode is miniscule. Although decaying with time, r remains in excess of 2 for up to 150 μs from the onset of the pump pulse, implying that the intrinsic limit on the maser amplifier's residual noise temperature stays below 140 mK for the same amount of time. Whether or not r can be sustained sufficiently above 1 to allow continuous maser operation (given a suitable pump source and adequate cooling) would seem to be finely balanced with respect to the values of the relevant relaxation parameters.

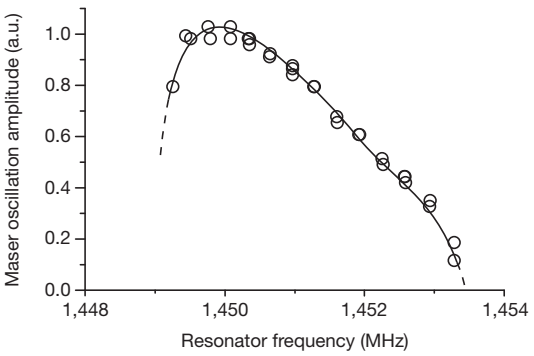

Figure 4 | Frequency response of maser action. The circles and associated guide line plot the measured plateau amplitude of the maser oscillation (vertical scale, obtained by down-converting the oscillation's output to a few tens of kilohertz and observing the resultant beat on a digital storage oscilloscope; a.u., arbitrary units) on illuminating the pentacene:*p*-terphenyl crystal (within its sapphire ring) with a ~0.5-J pulse of yellow light, for different frequencies of the microwave resonator's $TE_{01\delta}$ mode (horizontal scale).

When down-converted, sampled and Fourier-transformed, each burst of maser oscillation had a linewidth of ~6 kHz, consistent with that of a perfect sine wave modulated by the maser burst's envelope (Fig. 3, blue and green curves). Precise measurements of the maser's noise will be done if and when continuous operation is achieved.

With this device, we have demonstrated zero-field maser operation at room temperature with a solid-state gain medium. By improving the quality of the maser crystal, the effectiveness of the optical pumping and the Purcell factor of the resonator, we believe that the maser's threshold pump power can be substantially reduced, its efficiency (and, hence, output power as an oscillator) further increased and its residual noise temperature as an amplifier reduced. The application of a d.c. magnetic field bias should allow the maser's operating frequency to be tuned somewhat. The prospect of continuous maser operation, although not resolved here, remains a possibility and motivates attempts to identify different (yet perhaps structurally related) molecular systems whose properties are yet more advantageous for masing than those of pentacene:*p*-terphenyl.

Extremely low-noise amplifiers allow the detection of weak yet potentially important electromagnetic signals, which would otherwise go unnoticed. Low-phase-noise oscillators are essential components within frequency standards and clocks. Ultrasensitive parametric probes and detectors can, moreover, be derived from such oscillators. Because it can be operated at room temperature and in weak ambient magnetic fields (such as Earth's), the maser reported here thus opens new routes to the making of measurements at unprecedented levels of sensitivity and precision in areas such as space exploration, molecular biology and quantum computing. Furthermore, the general exploitation of intersystem crossing as an effective source of spin-polarized 'fuel' for the powering of more intricately orchestrated quantum molecular processes (beyond merely that of masing through a common microwave field) would seem to be a most fertile area of study.

METHODS SUMMARY

The maser crystal was grown using the vertical Bridgman–Stockbarger method in a double-walled glass vial[28]. Its constituent *p*-terphenyl was moderately zone-refined before growth; the substitutional concentration of its pentacene dopant was approximately 0.01%. The as-grown crystal boule was trimmed and then polished. It had extensive twinning (as revealed by spatially inhomogeneous birefringence) and other internal flaws (Fig. 2).

The microwave resonator was designed using both mode-matching and finite-element-method[29] software. The optical (*c*) axis of its monocrystalline sapphire ring lay parallel to the ring's geometric axis of rotation to within a tolerance of ±1°. All of the ring's surfaces and the internal surfaces of the resonator's silver-plated metal can were polished. On inserting the pentacene:*p*-terphenyl boule into the ring, the X↔Z transition was initially located by directly monitoring on an oscilloscope the response of an L-band Robinson oscillator bridge (which incorporated the resonator within its microwave circuit) to pulses of below-threshold yellow pump light.

The spin populations in the triplet ground state's X and Z sublevels, together with the photon number in the 1.45-GHz $TE_{01\delta}$ microwave mode, were modelled by coupled linear rate equations capturing the processes of stimulated emission and absorption, spin–lattice relaxation, and intersystem-crossing-mediated population into, and decay out of, the triplet sublevels[30]; see Methods for further details, including estimates of parameters that enter these equations as coefficients.

The predicted noise performance of our maser is based on formulae derived in ref. 5, which have previously been applied without low-temperature approximations to cryogenic ruby masers[6]. Noise contributions associated with losses in passive microwave components (including the resonator), as well as the 'intrinsic' maser noise associated with the effective spin temperature across the X↔Z transition, are all included in our analysis.

Full Methods and any associated references are available in the online version of the paper.

Received 30 March; accepted 18 June 2012.

1. Schawlow, A. L. & Townes, C. H. Infrared and optical masers. *Phys. Rev.* **112,** 1940–1949 (1958).

2. Maiman, T. H. Stimulated optical radiation in ruby. *Nature* **187,** 493–494 (1960).
3. Kleppner, D., Goldenberg, H. M. & Ramsey, N. F. Properties of the hydrogen maser. *Appl. Opt.* **1,** 55–60 (1962).
4. Konoplev, I. V. *et al.* Experimental study of coaxial free-electron maser based on two-dimensional distributed feedback. *Phys. Rev. Lett.* **96,** 035002 (2006).
5. Siegman, A. E. *Microwave Solid-State Masers* (McGraw-Hill, 1964).
6. Clauss, R. C. & Shell, J. S. Ruby masers. In *Low-Noise Systems in the Deep Space Network* (ed. Reid, M. S.) (Deep Space Communication and Navigation Series, Jet Propulsion Laboratory, Caltech, 2008).
7. Dick, G. J. & Wang, R. T. Ultra-stable performance of the superconducting cavity maser. *IEEE Trans. Instrum. Meas.* **40,** 174–177 (1991).
8. Bourgeois, P.-Y. *et al.* Maser oscillation in a whispering-gallery-mode microwave resonator. *Appl. Phys. Lett.* **87,** 224104 (2005).
9. Mollier, J. C., Hardin, J. & Uebersfeld, J. Theoretical and experimental sensitivities of ESR spectrometers using maser techniques. *Rev. Sci. Instrum.* **44,** 1763–1771 (1973).
10. van der Waals, J. H. EPR of photo-excited triplet states: a personal account. *Appl. Magn. Reson.* **20,** 545–561 (2001).
11. Sloop, D. J., Yu, H.-L., Lin, T.-S. & Weissman, S. I. Electron spin echoes of a photoexcited triplet: pentacene in *p*-terphenyl crystals. *J. Chem. Phys.* **75,** 3746–3757 (1981).
12. Köhler, J., Brouwer, A. C. J., Groenen, E. J. J. & Schmidt, J. On the intersystem crossing of pentacene in *p*-terphenyl. *Chem. Phys. Lett.* **250,** 137–144 (1996).
13. Bogle, G. S. & Symmons, H. F. Zero-field masers. *Aust. J. Phys.* **12,** 1–20 (1959).
14. Whelehan, J. J. Low-noise amplifiers—then and now. *IEEE Trans. Microw. Theory Tech.* **50,** 806–813 (2002).
15. Wadefalk, N. *et al.* Cryogenic wide-band ultra-low-noise IF amplifiers operating at ultra-low DC power. *IEEE Trans. Microw. Theory Tech.* **51,** 1705–1711 (2003).
16. Smith, B. A. *et al.* A new look at the Saturn system: the Voyager 2 images. *Science* **215,** 504–537 (1982).
17. Asztalos, S. J. *et al.* SQUID-based microwave cavity search for dark-matter axions. *Phys. Rev. Lett.* **104,** 041301 (2010).
18. Korolev, A. M., Shnyrkov, V. I. & Shulga, V. M. Ultra-high frequency ultra-low dc power consumption HEMT amplifier for quantum measurements in millikelvin temperature range. *Rev. Sci. Instrum.* **82,** 016101 (2011).
19. Blank, A., Kastner, R. & Levanon, H. Exploring new active materials for low-noise room-temperature microwave amplifiers and other devices. *IEEE Trans. Microw. Theory Tech.* **46,** 2137–2144 (1998).
20. Hsu, H. & Tittel, F. K. Optical pumping of microwave masers. *Proc. IEEE* **51,** 185–189 (1963).
21. Sabisky, E. S. & Anderson, C. H. A solid-state cw optically pumped microwave maser. *Appl. Phys. Lett.* **8,** 298–300 (1966).
22. Blank, A. & Levanon, H. Toward maser action at room temperature by triplet-radical interaction and its application to microwave technology. *RIKEN Rev.* **44,** 128–130 (2002).
23. Blank, A. & Levanon, H. Applications of photoinduced electron spin polarization at room temperature to microwave technology. *Appl. Phys. Lett.* **79,** 1694–1696 (2001).
24. Antipov, S. *et al.* in *Proc. 23rd Particle Accelerator Conf.* 4535–4537, https://accelconf.web.cern.ch/accelconf/PAC2009/papers/fr5rfp001.pdf (Joint Accelerator Conference Website, 2009).
25. Kagawa, A., Murokawa, Y., Takeda, K. & Kitagawa, M. Optimization of ^{1}H spin density for dynamic nuclear polarization using photo-excited triplet electron spins. *J. Magn. Reson.* **197,** 9–13 (2009).
26. Purcell, E. M. Spontaneous emission probabilities at radio frequencies. *Phys. Rev.* **69,** 681–686 (1946).
27. Lang, J., Sloop, D. J. & Lin, T.-S. Orientational anisotropic studies by field rotation technique: near zero-field pulsed EPR experiments of pentacene in *p*-terphenyl. *J. Magn. Reson.* **176,** 249–256 (2005).
28. Selvakumar, S. *et al.* Growth and studies on SSVBT grown *p*-terphenyl single crystals. *J. Cryst. Growth* **275,** e265–e271 (2005).
29. Oxborrow, M. Traceable 2-D finite-element simulation of the whispering-gallery modes of axisymmetric electromagnetic resonators. *IEEE Trans. Microw. Theory Tech.* **55,** 1209–1218 (2007).
30. Takeda, K., Takegoshi, K. & Terao, T. Zero-field electron spin resonance and theoretical studies of light penetration into single crystals and polycrystalline material doped with molecules photoexcitable to the triplet state via intersystem crossing. *J. Chem. Phys.* **117,** 4940–4946 (2002).

Acknowledgements M.O. thanks J. Sherwood, R. Ferguson and C. Langham for advice on the growth of molecular crystals, for help in cutting and polishing the crystalline *p*-terphenyl boule and for designing the metal components of the microwave resonator, respectively. M.O. and J.D.B. thank C. Kay for discussions and guidance on pulsed electron paramagnetic resonance spectroscopy. This work was supported by the NMS Pathfinder Metrology Programme and by the Engineering and Physical Sciences Research Council.

Author Contributions J.D.B. performed initial pulsed electron paramagnetic resonance experiments with M.O., and analysed the resultant data. Both J.D.B. and M.O. carried out independent electromagnetic modelling of the $TE_{01\delta}$-mode microwave resonator using different software. M.O. grew the pentacene:*p*-terphenyl crystal, designed and constructed the microwave circuitry and optical systems, performed the final experiments and analysed the resultant data. N.M.A. initiated the original work on high-*Q* cavities. N.M.A. and M.O. wrote the paper.

Author Information Reprints and permissions information is available at www.nature.com/reprints. The authors declare no competing financial interests. Readers are welcome to comment on the online version of this article at www.nature.com/nature. Correspondence and requests for materials should be addressed to M.O. (mo@npl.co.uk) or N.M.A. (n.alford@imperial.ac.uk).

METHODS

Maser crystal. The pentacene was of commercial origin and was donated by Sandrine Heutz of the Department of Materials, Imperial College London. The *p*-terphenyl was purchased from Alfa Aesar (99+% grade) and then moderately zone-refined, that is, sealed in glass tubes under dry argon and swept repeatedly at 0.5 mm min^{-1} up through a vertical furnace. A double-walled[28] vial of borosilicate glass (internal diameter, 18 mm; height, 70 mm; made by Cambridge Glassblowing Ltd) was charged with a mixture of pentacene and zone-refined *p*-terphenyl in a stoichiometric ratio of approximately 1:10^4. Owing to oxygen contamination during growth, the actual concentration of pentacene surviving in the crystal may have been somewhat lower than this. The vial was lowered through a vertical tube furnace at a rate of 1 mm h^{-1}. Although a clean, pink crystal formed initially, on cooling to room temperature at a rate of approximately 50 °C h^{-1}, many flaws appeared within it due to twinning and/or thermal shock. The vial was carefully cracked open and the crystal boule removed intact from it. This boule was then gently cut ('topped and tailed') with a circular saw and then polished, the last abrasive being opaline. The *p*-terphenyl crystal's *a*–*b* cleavage plane contained the boule's rotation axis to within ±5°. Extensive twinning meant that the crystal's *a* and *b* axes were differently oriented in different parts of the crystal (the pump beam always illuminated several such domains).

Microwave resonator. The resonator's basic aspect ratios and dimensions were modelled using in-house-written mode-matching software, with the aim of realizing a high-*Q* mode at 1.45 GHz. A '2.5-dimensional' FEM-based electromagnetic mode simulator[29] running in COMSOL, in conjunction with AutoCAD, was additionally used to determine suitable shapes and dimensions for all components. The polished sapphire ring was sourced from SurfaceNet GmbH. The metal can (including piston) was plated with a 30-μm layer of non-bright silver at Platerite (Aldershot, UK) and then polished by hand.

Modelling of the spin dynamics. We assume that the spin populations in the triplet ground state's X and Z sublevels, and the photon number in the 1.45-GHz $TE_{01\delta}$ microwave mode, are governed by coupled linear rate equations, with terms capturing the processes of stimulated emission and absorption, spin–lattice relaxation, and intersystem crossing-mediated population into, and decay out of, the triplet sublevels. (The Y sublevel is not included in the model as this would have introduced several more free parameters.) We ignore both the spatial variation of the $TE_{01\delta}$ mode's magnetic field across the pumped region of the pentacene:*p*-terphenyl crystal and the vectorial complexities associated with differently oriented pentacene molecules at different *p*-terphenyl lattice sites, in relation to the directions of both the (at least initially unpolarized) pump beam and the $TE_{01\delta}$ mode's magnetic field. Elaborations necessary to include the effects of inhomogeneous broadening and spin diffusion are not included; we assume a simple Lorentz-broadened X↔Z transition. We estimate that, owing to the large diameter of the pump beam and the low concentration of pentacene within the maser crystal (so increasing its absorption depth to the pump light), the heat generated by a single pump pulse shifts the frequency of the X↔Z transition by only a small fraction of its linewidth; we thus ignore thermal effects.

We have estimated (in part on the basis of a measurement using an optical power meter placed inside the sapphire ring) that, owing to reflections and scattering off poorly polished surfaces, only about 60% of the pump laser's output gets absorbed by the maser crystal; this optical loss is included in our model. On further assuming that the value for the room-temperature intersystem crossing yield is 62.5% (ref. 30) and that the values of the intersystem crossing population ratios ($p_X^{ISC}=0.76, p_Z^{ISC}=0.08$) and the decay lifetime of the Z sublevel ($\tau_Z=10^{-3}$ s) are those determined in ref. 11 from X-band spin-echo measurements, we estimate that the ratio of the decay lifetimes between the Z and X sublevels is $\tau_Z/\tau_X \approx 8.5$, that the effective linewidth of the X↔Z transition is $\Delta f \equiv 1/\pi T_2 \approx 860$ kHz and that the spin–lattice relaxation time is $T_1 \approx 135$ μs, with uncertainties of ±20% in all three parameters. These were the only free parameters fitted.

The green curve in Fig. 3 is the model prediction for the above parameter values. Our estimate of the linewidth agrees with the value of 700 kHz reported in ref. 27, and is broadly consistent with an estimate for the spin–spin relaxation time of $T_2 \approx 260$ ns extracted from a preliminary measurement on a small, more concentrated polycrystalline sample of pentacene:*p*-terphenyl using a standard X-band pulsed electron paramagnetic resonance spectrometer. Figure 4 would suggest, however, that our imperfect maser crystal suffers additional inhomogeneous broadening of a few megahertz. Our estimates of τ_Z/τ_X and T_1 are factors of two lower and several higher, respectively, when compared with the values of their high-magnetic-field counterparts, as determined in ref. 11. We have yet to study the zero-field Y↔Z and X↔Y transitions at ~1.34 GHz and ~107 MHz, respectively (the second requires a different sort of resonator suitable for VHF), as would be needed to determine all of the parameters within a complete model of the spin dynamics, including transitions to and from the Y sublevel.

Amplifier residual noise temperature. Configured as a cavity amplifier operated in reflection through a circulator, the maser's residual noise temperature can be formulated[5,6] as

$$T_{\text{noise}} = (1+1/G)\frac{L_{\text{circ.}}^{\text{dB}}}{e^{\text{dB}}}T_0 + (1-1/G)\left[\frac{L_{\text{cav.}}^{\text{dB}}}{G^{\text{dB}}}T_0 + \frac{G_{\text{mas.}}^{\text{dB}}}{G^{\text{dB}}}\frac{r}{r-1}\frac{hf_{\text{mas.}}}{k}\right] \quad (1)$$

where $X^{\text{dB}} \equiv 10\log_{10}(X)$ denotes a quantity's decibel equivalent ($e^{\text{dB}} \approx 4.343$); $L_{\text{circ.}}^{\text{dB}}$ is the insertion loss through the circulator; $G^{\text{dB}} \equiv G_{\text{mas.}}^{\text{dB}} - L_{\text{cav.}}^{\text{dB}}$ is the amplifier's overall logarithmic power gain, where $G_{\text{mas.}}^{\text{dB}}$ is the gain associated with the masing process and $L_{\text{cav.}}^{\text{dB}}$ is the passive loss of the 'dark' (unpumped) cavity in reflection; T_0 is the operational temperature of the cavity and circulator, taken here to be 293 K; $f_{\text{mas.}} \approx 1.45$ GHz; and $r \equiv N_X/N_Z$ is the spin population ratio between the uppermost (X) and lowest (Z) maser levels. We now assume that the amplifier is good; that is, that its power gain $G \gg 1$ and that $G_{\text{mas.}}^{\text{dB}} \gg L_{\text{cav.}}^{\text{dB}}$. By using a low-loss circulator of say $L_{\text{cav.}}^{\text{dB}} \approx 0.1$dB, the first term in equation (1) can be reduced to ~7 K. The middle term (proportional to $L_{\text{cav.}}^{\text{dB}}/G^{\text{dB}}$) originates in ohmic and/or dielectric losses in the cavity. When set to its maximum output power, the pump laser used in our experimental maser can provide sufficient light to exceed the masing threshold by a factor of approximately 50, that is, $L_{\text{cav.}}^{\text{dB}}/G^{\text{dB}} \approx 0.02$, giving the middle term a value of around 6 K; this noise contribution could be reduced further by devising a cavity with a higher magnetic Purcell factor or using a laser that supplies pulses of higher instantaneous pump power (though probably of only shorter duration).

This leaves the last, 'intrinsic' term in equation (1), which is proportional to $r/(r-1)$. The advantage of pumping optically via intersystem crossing is that *r* can be considerably greater than 1 even at room temperature. Naively taking this ratio to be that of the intersystem crossing process (Fig. 1) alone, that is, $r = 0.76/0.08 = 9.5$, the intrinsic term contributes a noise temperature of just 78 mK. In reality, *r* will be reduced by relaxation processes as time increases (Fig. 3, red curve), so raising this noise temperature. But the maser amplifier's overall noise temperature may still be deeply cryogenic for long enough to render the amplifier advantageous in certain pulse-mode applications such as the amplification of radar echoes. Various improvements are possible here, such as the construction of a travelling-wave maser[5,6], which would obviate the circulator's up-front noise contribution, in a narrow yet low-loss ('slow-wave') waveguide to keep $L_{\text{cav.}}^{\text{dB}}/G^{\text{dB}}$ low.